

A semi-parametric model for ice accumulation rate and temperature based on Antarctic ice core data

Radhendushka Srivastava
Department of Mathematics, IIT Bombay India
and
Debasis Sengupta
Applied Statistics Unit, ISI Kolkata, India

September 8, 2023

Abstract

In this paper, we present a semiparametric model for describing the effect of temperature on Antarctic ice accumulation on a paleoclimatic time scale. The model is motivated by sharp ups and downs in the rate of ice accumulation apparent from ice core records, which are synchronous with movements of temperature. We prove strong consistency of the estimators under reasonable conditions. We conduct extensive simulations to assess the performance of the estimators and bootstrap based standard errors and confidence limits for the requisite range of sample sizes. Analysis of ice core data from two Antarctic locations over several hundred thousand years show a reasonable fit. The apparent accumulation rate exhibits a thinning pattern that should facilitate the understanding of ice condensation, transformation and flow over the ages. There is a very strong linear relationship between temperature and the apparent accumulation rate adjusted for thinning.

Keywords: Nonlinear regression; strong consistency; kernel smoothing; model based bootstrap; dependent errors.

1 Introduction

An important question in the context of climate change is how the global stocks of frozen water at high elevations and the polar regions would hold up against the warming climate. Reports of melting glaciers from various parts of the planet have raised the stakes for the answer to this question in respect of the largest mass of ice, namely the Antarctic ice sheet. While there is empirical evidence (Allan and Soden, 2008; Algarra *et al.*, 2020) as well as theoretical explanations (Wang, 2013) of greater transportation of moisture in the atmosphere resulting from higher temperatures, there is no clear evidence of the same translating into excess precipitation that can offset the loss of ice from the Antarctic continent. Recent claims of such an offset based on satellite radar and laser altimetry (Zwally *et al.*, 2015) have since been contested (Scambos and Shuman, 2016). A major source of confusion in this regard is the large margin of error in altimetry based estimates. Here we look for an answer from the climatological history of the Earth over several hundred thousand years.

Ice core data records are the only source of information on the long term linkage between temperature and ice accumulation. It is important to note that the reconstructed age and temperature corresponding to a specific ice core are based on concentration of isotopic elements extracted in the laboratory. These data sets are prone to error, which may occur during the process of extraction of isotopic material as well as reconstruction of age and temperature of the ice cores. There is added complication arising from adjustments of reconstructed ages for alignment with the available domain knowledge. Further, ever since a layer of ice is formed, it goes through a process of thinning under the weight of subsequently deposited layers. A relationship between temperature and ice accumulation over the years needs a careful investigation that takes into account the thinning of ice sheets.

In this article, we explore this relationship by using ice core data from two locations in Antarctica, Lake Vostok and Dome C of the European Project for Ice Coring in Antarctica (EPICA). The temperature of the different slices of the ice cores is estimated from the concentration of Deuterium isotopes present in the core using dating techniques. The ages of the ice layers at Lake Vostok and EPICA Dome C were originally documented in the GT4 scale (Petit *et al.*, 1999) and the EDC3 scale (Parrenin *et al.*, 2007), respectively. The GT4 scale utilizes an ice flow model (aided by isotopic stratigraphic control points at 1534 m (110 kyr) and at 3254 m (390 kyr)) under the assumption that the rate of accumulation of ice varies proportionally to the derivative of the water vapour saturation pressure, which is itself dependent on temperature (Siegert, 2003). This procedure may be susceptible to inducing distortions of the role of temperature. The EDC3 scale is also closely related. In order to avoid this possibility, we use for both the data sets the AICC2012 time scale, which is more broadly based (Bazin *et al.*, 2013).

For ice core data, the temperature anomaly, which is the deviation from long term average temperature, is reported in degree Celsius, and the age of ice cores is expressed in Kilo Years Before Present (KYrBP, the “present” being the year 1950). An overview of the two data sets, compiled for uniform intervals of depth, is given in Table 1.

The age difference at successive depths indicates the number of kilo years of net ice accumulation represented by the particular range of depths. We define the apparent accumulation rate (AAR) as the ratio of the height difference of successive ice core samples (measured in meters) and the age difference (in KYrBP) of these samples, as a function of the average age of the two successive layers (in KYrBP). Let d_i , a_i , and t_i denote the depth, the age and the temperature anomaly, respectively, of the i th observation of the ice core for $i = 1, 2, \dots, n + 1$, where $n + 1$ is the total number of observations. The AAR over

Table 1: Overview of the two ice core data sets (Petit *et al.*, 1999; Jouzel and Masson-Delmotte, 2007; Rapp, 2019)

Location	Age limit (KYrBP)	Depth limit (meters)	Base altitude above MSL (meters)	Sample size	Sampling interval (meters)
Lake Vostok (77°50'S 106°00'E)	403.780	3263	-500	3311	1.00
EPICA Dome C (75°06'S 123°20'E)	801.588	3189.45	-40	5800	0.55

the age interval (a_i, a_{i+1}) , represented by the average age $z_i = (a_i + a_{i+1})/2$, is

$$b_i = \frac{d_{i+1} - d_i}{a_{i+1} - a_i}, \quad i = 1, 2, \dots, n. \quad (1)$$

This rate corresponds to the age z_i and the average of the temperature anomalies at the endpoints of the slice intervals, i.e., $x_i = (t_i + t_{i+1})/2$ (henceforth referred to as ‘temperature’).

Figure 1 shows the plots of temperature (on the left vertical axis) and AAR (in log scale, on right vertical axis) against age at the two locations. The plots indicate that the fluctuations of AAR with those of the temperature move in the same direction together with a general long term decreasing trend in AAR for both the data sets.

The reason for our focus on the *apparent* accumulation rate is that the actual rate of ice accumulation cannot be observed over a paleo-climatic scale of age. AAR is the net accumulation observed on site today as the overall effect of several factors like precipitation, thinning under the pressure from the weight of ice lying above (compression factor) through relocation/expulsion of gas and water molecules trapped in ice, and lateral flow of ice.

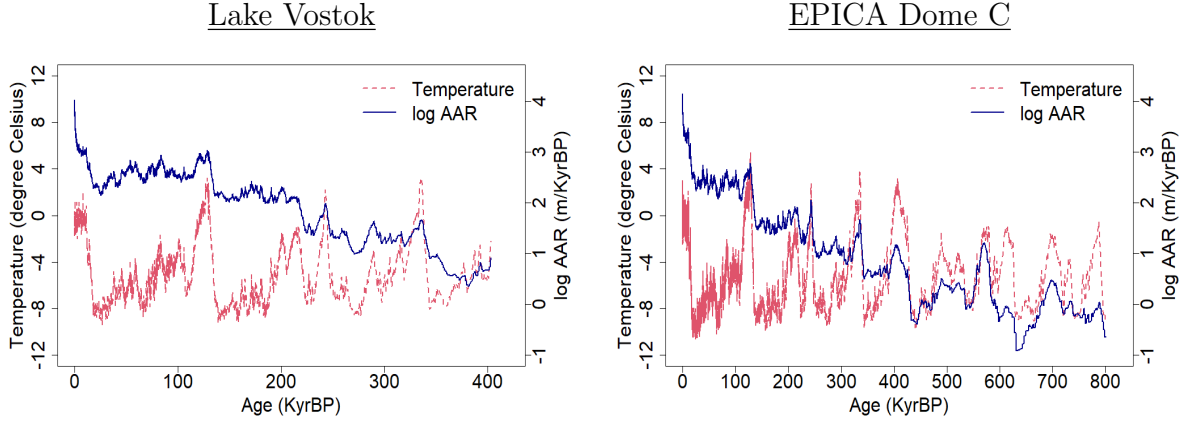


Figure 1: The plots of temperature (in $^{\circ}\text{C}$, red curve, labeled along the left vertical axis) and logarithm of AAR (in m/KYr , blue curve and labeled along the right vertical axis) versus age (KYrBP)

There have been efforts to delineate the actual accumulation rate from thinning, and the results of that exercise are available in the public domain (<https://www.ncei.noaa.gov/access/paleo-search/study/15076>). We choose not to separate the two, so as to avoid unnecessary imprecision in assessing the linkage between temperature and accumulation.

In Section 2, we present a multiplicative model for AAR that combines a decreasing function of age with a factor that depends linearly on the temperature. We also present an algorithm for estimating the parameters. In Section 3, we establish strong consistency of the estimators under appropriate conditions. In Section 4, we provide a model based bootstrap method to estimate the standard error and the confidence limits of the parameters. In Section 5, we report the findings of a simulation study to validate the applicability of the theoretical results as well as the bootstrap method to the requisite sample size. In Section 6, we present the analysis of both the ice core data sets and discuss the implications of the findings. Proofs of all the theoretical results are given in the Appendix.

2 The model and the method

We aim to capture the movement of AAR, observed in Figure 1, by the semi-parametric and multiplicative model

$$b_i = (1 + \gamma_0 x_i) g_0(z_i) \xi_i, \quad \text{for } i = 1, 2, \dots, n, \quad (2)$$

where γ_0 is the parameter associated with the temperature (x), g_0 is a decreasing function of the age (z) and ξ is a sequence of positive valued disturbance term.

In the model (2), the AAR and temperature are related in a linear manner. The parameter γ_0 is the rate of increase in AAR with 1°C rise in temperature. The function g_0 is meant to capture the long term decreasing trend visible in AAR (see Figure 1). We regard the function g_0 as a nuisance parameter that represents the nominal rate of accumulation at temperature $x = 0$, subject to thinning. Specifically, the thinning factor at a specific age z is $g_0(z)/g_0(0)$. The disturbance term ξ represents the possible error in indirect measurements, and various other atmospheric phenomenon that affect AAR but not included in the model (2).

By allowing g_0 to be a general decreasing function, we are able to free the analysis from uncertainties in the determination of age. As mentioned in the foregoing section, there have been multiple attempts to determine the scale of age accurately. The different scales of age may be regarded as monotonically increasing transformations of one another that preserve the order among ages estimated for successive slices of the ice core. Some amount of error in the determination of age is expected. Any such error cannot alter the form of the model (2), where g_0 continues to be a decreasing function of the estimated age.

We consciously left out an intercept parameter from the linear factor of the model (2). Inclusion of an intercept parameter leads to confounding of the linear factor with g_0 . An alternative way of ensuring identifiability of the model is to impose a boundary condi-

tion like $g_0(0) = 1$, which makes g_0 the thinning factor. However, that strategy would make all the estimators vulnerable to the well known issues of functional estimation at the boundaries (Härdle, 1990).

The log transformation of model (2) produces the additive semiparametric model

$$y_i = \log(1 + \gamma_0 x_i) + \log g_0(z_i) + \varepsilon_i, \quad i = 1, 2, \dots, n, \quad (3)$$

where $y_i = \log b_i$ and $\varepsilon_i = \log \xi_i$. The values of AAR at successive slices of the ice core make use of common values of depth and age at the boundary. This construction induces dependence in the AAR sequence. Dependence is also expected to arise from the use of the AICC2012 scale of age, where the ages are subjected to the constraint of monotonicity and are calibrated with other information. In order to address this dependency, we model the noise sequence ε as an autoregressive process (see Assumption 3 below). Sreelekshmy (2023) studied a similar model for ice accumulation under the assumption of independently and identically distributed errors.

The parameters of model (3) are estimated by minimizing the average squared error loss function

$$Q_n(\gamma, g) = \frac{1}{n} \sum_{i=1}^n (y_i - \log(1 + \gamma x_i) - \log g(z_i))^2, \quad (4)$$

with respect to the scalar parameter γ and the functional parameter g . The optimization is made over the space $\Gamma \times \mathcal{G}$, where $\Gamma = [-1/x^{(M)}, 1/x^{(m)}]$, $x^{(m)}$ and $x^{(M)}$ being positive numbers satisfying $-x^{(m)} < x < x^{(M)}$ for all x (so that $(1 + \gamma x) > 0$ for $\gamma \in \Gamma$), and

$$\begin{aligned} \mathcal{G} = \{g \in C[0, A] : g \text{ is positive valued, non-increasing function} \\ \text{with uniformly bounded left and right derivatives}\}, \quad (5) \end{aligned}$$

A being a positive number larger than the oldest age of ice. The parameter of main interest is γ , while g is a nuisance parameter.

An iterative two stage coordinate descent algorithm is adapted for minimizing Q_n with respect to γ and $\log g$. The initial iterate for γ is $\hat{\gamma}_n^{(0)} = 0$. Substitution of this value in (4) leads to the initial iterate of g ,

$$\log \hat{g}_n^{(0)} = \arg \min_{g \in \mathcal{G}} \frac{1}{n} \sum_{i=1}^n (y_i - \log g(z_i))^2. \quad (6)$$

The values of $\log \hat{g}_n^{(0)}$ at the requisite points may be written explicitly as

$$\log \hat{g}_n^{(0)}(z_i) = \min_{1 \leq j \leq i} \max_{i \leq l \leq n} \frac{y_j + \dots + y_l}{l - j + 1}, \quad (7)$$

and obtained by the pool-adjacent-violators algorithm (PAVA). The k^{th} iterate of γ is

$$\hat{\gamma}_n^{(k)} = \arg \min_{\gamma \in \Gamma} \frac{1}{n} \sum_{i=1}^n (y_i - \log \hat{g}^{(k-1)}(z_i) - \log(1 + \gamma x_i))^2 \quad k \geq 1. \quad (8)$$

The Gauss-Newton algorithm is used to minimize (8). The k^{th} iterate of g is

$$\log \hat{g}_n^{(k)} = \arg \min_{g \in \mathcal{G}} \frac{1}{n} \sum_{i=1}^n (y_i - \log(1 + \hat{\gamma}_n^{(k)} x_i) - \log g(z_i))^2, \quad k \geq 1, \quad (9)$$

where $\log \hat{g}_n^{(k)}$ is obtained by using PAVA on the sequence $y_i - \log(1 + \hat{\gamma}_n^{(k)} x_i)$, $i = 1, 2, \dots, n$.

The iterations (8) and (9) are carried out alternately. We denote the limiting values of $\hat{\gamma}_n^{(k)}$ and $\log \hat{g}_n^{(k)}$ by $\hat{\gamma}_n$ and $\log \hat{g}_n$, respectively, and presume linear interpolation of the latter in between the locations of estimation. The iterations are continued until the relative change in the average squared error loss criterion in successive iterations is less than the desired threshold.

As $\log g_0$ is presumed to be a smooth function, a smoothed version of the piecewise constant estimator $\log \hat{g}_n$ is desirable. We propose the kernel smoothed estimator

$$\log \tilde{g}_n(z) = \frac{\frac{1}{nh} \sum_{i=1}^n K\left(\frac{z-z_i}{h}\right) \log \hat{g}_n(z_i)}{\frac{1}{nh} \sum_{i=1}^n K\left(\frac{z-z_i}{h}\right)} \quad \text{for } z > 0, \quad (10)$$

where $K(\cdot)$ is the kernel function and h is the bandwidth. Based on $\log \tilde{g}_n$, we update the estimator of γ_0 as

$$\tilde{\gamma}_n = \arg \min_{\gamma \in \Gamma} \frac{1}{n} \sum_{i=1}^n (y_i - \log \tilde{g}_n(z_i) - \log(1 + \gamma x_i))^2. \quad (11)$$

3 Strong consistency of estimators

Note that Γ and \mathcal{G} are compact subsets of \mathbb{R} and $C[0, A]$, respectively. Consequently, the parameter space $\Gamma \times \mathcal{G}$ with the *product distance function*

$$d((\gamma_1, g_1), (\gamma_2, g_2)) = |\gamma_1 - \gamma_2| + \sup_{z \in [0, A]} |g_1(z) - g_2(z)| \quad \text{for } \gamma_1, \gamma_2 \in \Gamma \text{ and } g_1, g_2 \in \mathcal{G}$$

is a complete separable metric space. The existence of the estimators for such a parameter space follows from arguments similar to those in Jennrich (1969).

For proving almost sure convergence of the criterion and strong consistency of the estimators, we make some assumptions on the sequences of age (z), temperature (x), and errors (ε).

Assumption 1. *The numbers $z_1 < z_2 < \dots < z_n$ are the values of a continuous function $z(d)$ at uniformly spaced depths $0 = d_1 < d_2 < \dots < d_n = \Delta$ with $d_i = \frac{i\Delta}{n}$, for $i = 1, 2, \dots, n$ and Δ is a positive number.*

Assumption 2. *The numbers x_1, x_2, \dots, x_n lying within the interval $(x^{(m)}, x^{(M)})$ are the values of a continuous function $x(d)$ at uniformly spaced depths $0 = d_1 < d_2 < \dots < d_n = \Delta$ with $d_i = \frac{i\Delta}{n}$, for $i = 1, 2, \dots, n$ and Δ is a positive number.*

Assumption 3. *The error sequence $\{\varepsilon_i\}_{1 \leq i \leq n}$ is a zero mean and causal autoregressive process of order 1, following the recursive relation*

$$\varepsilon_i = \phi \varepsilon_{i-1} + U_i, \quad i = 2, 3, \dots, n,$$

where $0 < |\phi| < 1$, and the innovation $\{U_i\}_{1 \leq i \leq n}$ is a sequence of i.i.d. random variables with mean 0, variance σ^2 and $E(U_1^8) < \infty$.

Theorem 1. Under Assumptions 1-3, the average squared error loss function $Q_n(\gamma, g)$ defined in (4) converges uniformly to $Q(\gamma, g) + \frac{\sigma^2}{1-\phi^2}$ with probability 1 as $n \rightarrow \infty$, where

$$Q(\gamma, g) = \frac{1}{\Delta} \int_0^\Delta [\log(1 + \gamma_0 x(w)) - \log(1 + \gamma x(w)) + \log g_0(z(w)) - \log g(z(w))]^2 dw.$$

Note that $Q(\gamma, g) \geq 0$ for every $\gamma \in \Gamma$ and $g \in \mathcal{G}$ and that $Q(\gamma_0, g_0) = 0$.

Theorem 2. If $Q(\gamma, g)$ has a unique minimum at (γ_0, g_0) , and Assumptions 1-3 hold, then $(\hat{\gamma}_n, \hat{g}_n)$ converges almost surely to (γ_0, g_0) as $n \rightarrow \infty$.

In view of the fact that log is a monotone function, we have the following corollary to Theorem 2.

Corollary 1. If the conditions of Theorem 2 hold, then $\sup_z |\log \hat{g}_n(z) - \log g_0(z)|$ converges to 0 with probability 1.

For establishing almost sure convergence of the smoothed estimator, we make the following assumption on the kernel function.

Assumption 4. The kernel $K > 0$ is a differentiable function supported on $(-1, 1)$.

Theorem 3. Let g_0 be a positive valued and continuously differentiable function bounded away from 0. Then under Assumptions 1-4, as $h \rightarrow 0$ and $n \rightarrow \infty$, we have the following.

(i) $\sup_z |\log(\tilde{g}_n(z)) - \log(g_0(z))| \rightarrow 0$ almost surely.

(ii) $\tilde{\gamma}_n \rightarrow \gamma_0$ almost surely.

For the purpose of resampling, described in the next section, we have to estimate the error parameters mentioned in Assumption 3. By using the set of residuals

$$\tilde{\varepsilon}_i = y_i - \log(1 + \tilde{\gamma}_n x_i) - \log \tilde{g}_n(z_i), \text{ for } i = 1, 2, \dots, n, \quad (12)$$

we define the estimators of ϕ and σ^2 as

$$\tilde{\phi}_n = \frac{\frac{1}{n} \sum_{i=2}^n \tilde{\varepsilon}_i \tilde{\varepsilon}_{i-1}}{\frac{1}{n} \sum_{i=2}^n \tilde{\varepsilon}_i^2}, \quad (13)$$

$$\tilde{\sigma}_n^2 = \frac{1}{n} \sum_{i=2}^n \left(\tilde{\varepsilon}_i - \tilde{\phi}_n \tilde{\varepsilon}_{i-1} \right)^2. \quad (14)$$

The next theorem establishes the strong consistency of the estimators $\tilde{\phi}_n$ and $\tilde{\sigma}_n^2$ over the parameter spaces $(-1, 1)$ and $(0, \infty)$, respectively.

Theorem 4. *If the assumptions of Theorem 3 hold, then we have the following as $n \rightarrow \infty$.*

(i) $\tilde{\phi}_n \rightarrow \phi$ almost surely.

(ii) $\tilde{\sigma}_n^2 \rightarrow \sigma^2$ almost surely.

4 Bootstrap standard error and confidence limits

Nonparametric and model based bootstrap methods provide a computational alternative to the calculation of sampling distribution of estimators, for obtaining standard errors (Efron and Tibshirani, 1993) and confidence intervals (DiCiccio and Efron, 1996). While the bootstrap was originally proposed for independent and identically distributed data, model based methods for dependent data, pertinent for the present work, have been studied in subsequent literature (see Lahiri (2003)). An obstacle to model based bootstrap in the present case is the PAVA estimator for isotonic regression, which is known to lead to overfitting

(Niculescu-Mizil and Caruana, 2005; Luss *et al.*, 2012), and consequently to systematically underestimated magnitudes of residuals. For the analogous problem of monotonic density estimation, Sen *et al.* (2010) showed that the bootstrap confidence interval of the Grenander estimator is inconsistent, and provided a consistent procedure obtained by smoothing the Grenander estimator, which averts the pitfalls of resampling from excessively small residuals. It is for this reason that the smoothed nonparametric estimator $\log \tilde{g}_n$ was chosen for specification of variance by bootstrap.

The following are the suggested steps for generating model-based bootstrap replicates of $\tilde{\gamma}_n$ and $\log \tilde{g}_n$.

- (i) Estimate the innovation sequence as

$$\tilde{U}_i = \tilde{\varepsilon}_i - \tilde{\phi}_n \tilde{\varepsilon}_{i-1}, \text{ for } i = 2, 3, \dots, n,$$

where $\tilde{\varepsilon}_i$ and $\tilde{\phi}_n$ are as defined in (12) and (13), respectively.

- (ii) Draw an innovation sample of size n by using simple random sampling with replacement (SRSWR) from $\{\tilde{U}_i, i = 2, 3, \dots, n\}$ (see Chapter 2 of Lahiri (2003)), and denote it by $\{U_i^*, U_2^*, \dots, U_n^*\}$.
- (iii) If sample variance of $(U_i^*, i = 1, 2, \dots, n)$ is smaller than that of $\{\tilde{U}_i, i = 2, 3, \dots, n\}$, repeat step (ii). Else, proceed to the next step.
- (iv) Compute a bootstrap replicate of AAR from model (3) as

$$y_i^* = \log(1 + \tilde{\gamma}_n x_i) + \log \tilde{g}_n(z_i) + \tilde{U}_i^* - \tilde{\phi}_n \tilde{U}_{i-1}^*, \quad i = 2, \dots, n,$$

where $\tilde{\gamma}_n$ and $\log \tilde{g}_0$ are as defined in (11) and (10), respectively.

- (v) Estimate $\log \tilde{g}_0^*$ and $\tilde{\gamma}_n^*$ by substituting y_i^* in place of y_i in (10) and (11) respectively.

Step (iii) is a conservative measure meant to provide additional protection against overly small residuals for resampling. The above steps have to be repeated to produce the bootstrap replicates $\log \tilde{g}_0^*$ and $\tilde{\gamma}_n^*$ independently a large number of times. The bootstrap estimates of the standard errors of $\tilde{\gamma}_n$, and $\log \tilde{g}_n(z)$ are the sample standard deviations of the corresponding bootstrap replicates. For any given value of α , the middle $(1 - \alpha)\%$ of the relevant bootstrap replicates would constitute bootstrap confidence intervals of $\tilde{\gamma}_n$ and $\log \tilde{g}_n(z)$ for any z .

5 Simulation Study

In order to understand the finite sample performance of the methods presented in Sections 3 and 4, we run some simulations under conditions chosen to mimic the circumstances of the ice core data. The sequence of depths is presumed to be a uniform grid over the interval 0 to $\Delta = 3000$ meters, for sample sizes $n = 750, 1500, 3000$ and 6000 . The choices $n = 3000$ and $n = 6000$ are similar to the sample sizes of the ice core data from Lake Vostok and EPICA Dome C, respectively, and the other two choices extend the explored range of sample sizes. The grid spacing is $\frac{\Delta}{n}$. We choose the age z_i (in KYrBP) and temperature x_i (in degree Celsius) at depth $d_i = \frac{i\Delta}{n}$ as

$$\begin{aligned} z_i &= (7 \times 10^{-5}) d_i^2, \\ x_i &= -3 + 8 \cos(14\pi \times 10^{-7} d_i^2) + \vartheta_i, \end{aligned}$$

where $\vartheta_1, \dots, \vartheta_n$ are i.i.d. standard normal random variables, generated only once for all the simulation runs. These choices approximate the patterns of age and temperature observed in the two data sets. We choose the effect of temperature as $\gamma_0 = 0.05$ and the nominal accumulation rate at temperature $x = 0$ as the exponentially decaying function

$g_0(z) = 25 e^{-z/100} + 1$. We choose the parameters of the noise sequence ε as $\phi = 0.95$ and $\sigma^2 = 0.01$. For the kernel smoothed estimator $\log \tilde{g}_n$, we choose the Epanechnikov kernel

$$K(w) = \begin{cases} \frac{3}{4}(1 - w^2) & \text{if } |w| \leq 1 \\ 0 & \text{Otherwise.} \end{cases}$$

All the empirical measures of performance are computed on the basis of 1000 simulation runs. The bootstrap estimates reported in Sections 5.1 and 5.3 are based on 1000 sets of re-samples for each simulation run.

5.1 Choice of bandwidth

There are generic considerations for choosing the bandwidth h of the kernel function, which is the smoothing parameter (Härdle, 1990). However, generic considerations do not always work well in some specific situations (Ghosh and Chaudhuri, 2004). The focus of this article is on modeling and estimation of the effect of temperature on AAR for the ice core data, along with a reliable measure of its uncertainty. Therefore, we studied the coverage probability of bootstrap confidence intervals of γ at various choices of bandwidth h , and sought a bandwidth that can produce reasonable coverage under simulated conditions designed to match the circumstances of the data sets.

For this purpose, we simulated data sets as described above, fitted the model (3) and drew 1000 bootstrap samples from the residuals in the manner described in Section 4. As mentioned in that section, the range of the middle 95% of the bootstrap replicates of $\tilde{\gamma}_n$ is the bootstrap confidence interval of γ_0 with nominal coverage probability $1 - \alpha = 0.95$. We noted for each simulation run the actual inclusion status of the correct value of the parameter ($\gamma_0 = 0.05$), and repeated the process 1000 times. Figure 2 shows the proportion of times, out of these 1000 runs, that the bootstrap confidence interval included the correct

value of the parameter, for a range of values of h and sample sizes 750, 1500, 3000 and 6000. The values of h were varied over a coarse grid of size 10 over the interval $[0, 120]$ and a finer grid of size 1 over the interval $[20, 40]$. The limiting case $h = 0$ corresponds to no smoothing. The proportion of inclusion may be called the empirical coverage probability.

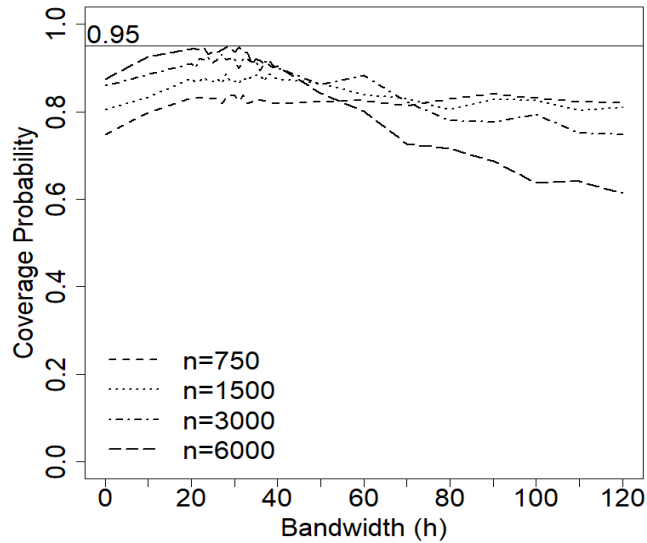


Figure 2: Plots of empirical coverage probability for γ_0 .

It is seen from Figure 2 that the empirical coverage probability is lower than the nominal coverage probability for smaller sample sizes. The plots feature a peak that gets narrower and approaches the nominal level as the sample size increases. There is not much shortfall in coverage for sample sizes 3000 and 6000. For all the sample sizes used in the simulations, there is an indication of maximum coverage over the range $h = 20$ to $h = 35$, though the peak is wider for sample sizes 3000 and below. We report the remaining results of the simulation study for the bandwidth $h = 28$, which is well inside this range.

5.2 Finite sample performance of estimators across runs

Table 2 shows the empirical bias and standard deviation (sd) of the estimators $\tilde{\gamma}_n$, $\tilde{\phi}_n$, and $\tilde{\sigma}_n^2$. Evidently, all the biases and standard deviations reduce with increase in the sample size, as one expects for consistent estimators. The bias is generally smaller in magnitude than the standard deviation, except in the case of $\tilde{\phi}_n$.

Table 2: Empirical bias and standard deviation (sd) of $\tilde{\gamma}_n$, $\tilde{\phi}_n$ and $\tilde{\sigma}_n^2$ based on 1000 simulation runs

n	bias: $\tilde{\gamma}_n$	sd: $\tilde{\gamma}_n$	bias: $\tilde{\phi}_n$	sd: $\tilde{\phi}_n$	bias: $\tilde{\sigma}_n^2$	sd: $\tilde{\sigma}_n^2$
750	-3.8×10^{-4}	5.0×10^{-3}	4.9×10^{-2}	2.1×10^{-2}	-8.8×10^{-5}	6.3×10^{-4}
1500	-2.5×10^{-4}	4.4×10^{-3}	-2.3×10^{-2}	1.1×10^{-2}	4.3×10^{-5}	4.5×10^{-4}
3000	1.0×10^{-4}	3.5×10^{-3}	-1.2×10^{-2}	6.8×10^{-3}	6.8×10^{-5}	3.3×10^{-4}
6000	5.0×10^{-5}	2.7×10^{-3}	-6.2×10^{-3}	4.5×10^{-3}	4.1×10^{-5}	2.1×10^{-4}

The left and right panel of Figure 3 show the plots of the estimates of pointwise bias and standard deviation, respectively, of the estimator $\log(\tilde{g}_n(z))$. Apart from the excessive errors at the boundaries, which is a well-known feature of nonparametric estimators of functions including isotonic regression estimators (Barlow *et al.*, 1972), the notable features of these plots are (a) smaller magnitude of bias than standard error and (b) reduction of both of these measures with increase in the sample size.

5.3 Finite sample performance of bootstrap method

Figure 4 shows the histograms of bootstrap estimates of the standard error of $\tilde{\gamma}_n$ for sample sizes $n = 750$ (top left) and $n = 1500$ (top right), $n = 3000$ (bottom left) and $n = 6000$ (bottom right), respectively. The estimate of standard error computed directly from

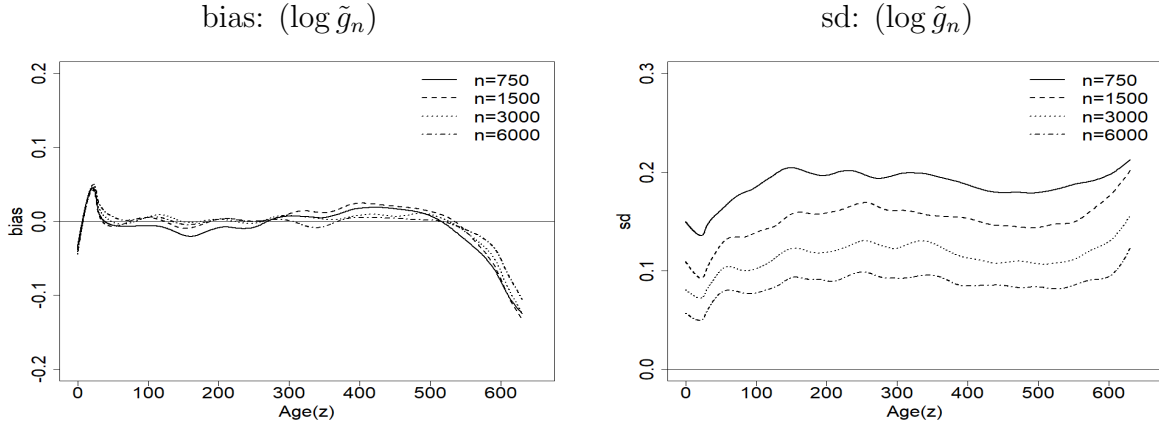


Figure 3: Plots of estimates of pointwise bias (left column) and sd (right column) of $\log(\tilde{g}_n(z))$.

the multiple simulation runs (without bootstrap) is shown as a maroon vertical line on each plot. The histograms reflect a general pattern of underestimation and a greater concentration of the bootstrap estimates around the maroon line for larger sample sizes. The empirical coverage probabilities of the bootstrap confidence interval (intended for 95% coverage), reported on the left side of each of the histograms, is close to the nominal coverage probability for larger sample sizes.

Figure 5 shows the empirical pointwise coverage probability of the bootstrap confidence intervals (with nominal coverage probability 0.95) of $\log g$. As the sample size increases, the pointwise coverage probabilities approach the nominal level. The coverage probabilities are lower than the nominal level around the boundaries even for larger sample sizes. This may have been due to excessive bias in the estimates in these areas, as observed in the section 5.2.

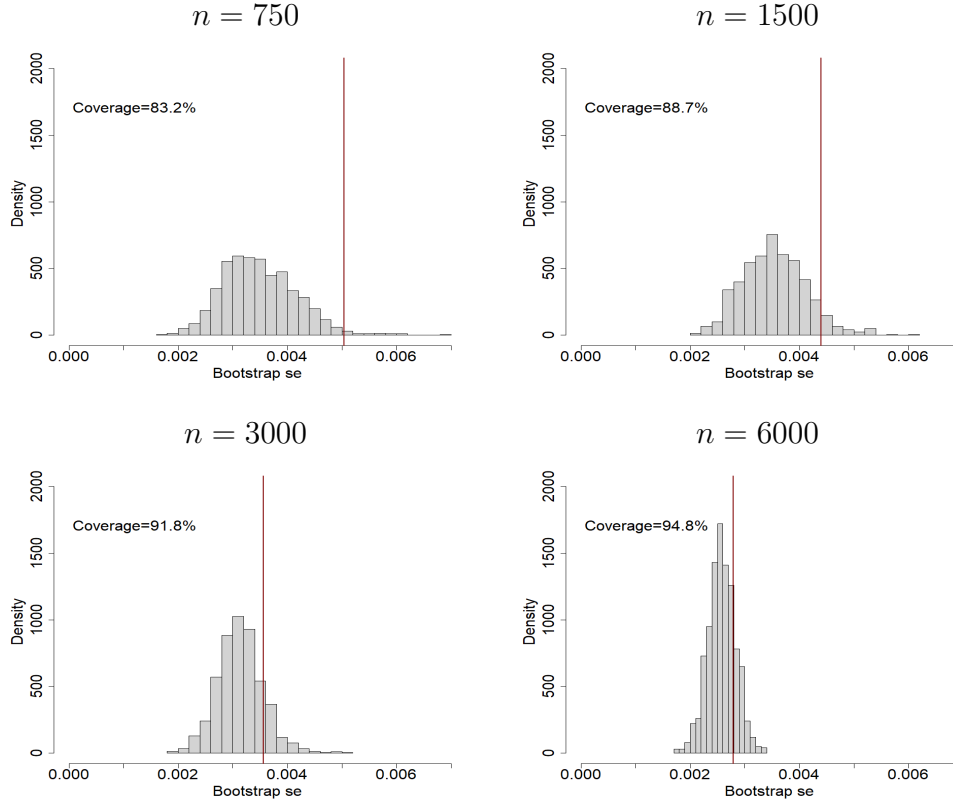


Figure 4: Histograms of bootstrap estimates of the standard error of $\hat{\gamma}_n$ and empirical coverage probability of nominally 95% coverage confidence intervals

6 Analysis of Lake Vostok and EPICA Dome C Data

For the analyses of the ice core data sets, we choose the Epanechnikov kernel with bandwidth $h = 28$, as in the simulations. The standard error of the estimators and the confidence limits are computed from 1000 bootstrap samples.

Table 3 shows the estimated value of parameter γ and its bootstrap standard error (s.e.) along with the bootstrap confidence interval (c.i.) for both locations. The table indicates

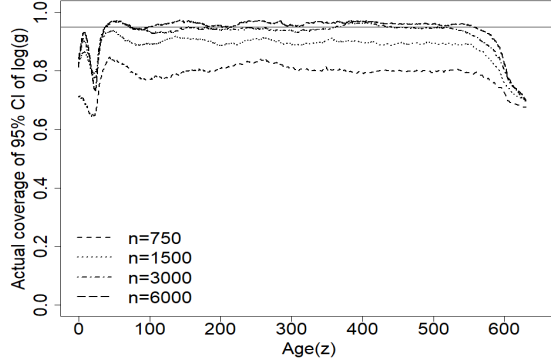


Figure 5: Plots of empirical coverage probabilities of the pointwise bootstrap confidence intervals of $\log g$.

that the value of γ for two locations are similar. The confidence interval is tighter in the case of EPICA Dome C, where the sample size is higher.

Table 3: Estimates of the γ with bootstrap s.e. and confidence interval.

Location	$\tilde{\gamma}_n$	Bootstrap s.e. ($\tilde{\gamma}_n$)	95% Bootstrap c.i. of γ
Lake Vostok	0.05779	0.00378	(0.04943, 0.06413)
EPICA Dome C	0.06191	0.00163	(0.05804, 0.06428)

The plots of observed and fitted values of $\log(\text{AAR})$ against Age for the two locations are shown in the top panel of Figure 6. The plots indicate that the proposed model (3) fits both the data sets reasonably well.

The plots of the estimated function $\log(\tilde{g})$ against age for the two locations, along with 95% pointwise confidence intervals, are shown in the middle panel of Figure 6. The plots suggest somewhat different thinning patterns at the two sites. This may have been caused not only by the differences in topography, but also by the fact that there is a lake underneath the ice sheet at one site and solid bedrock at the other.

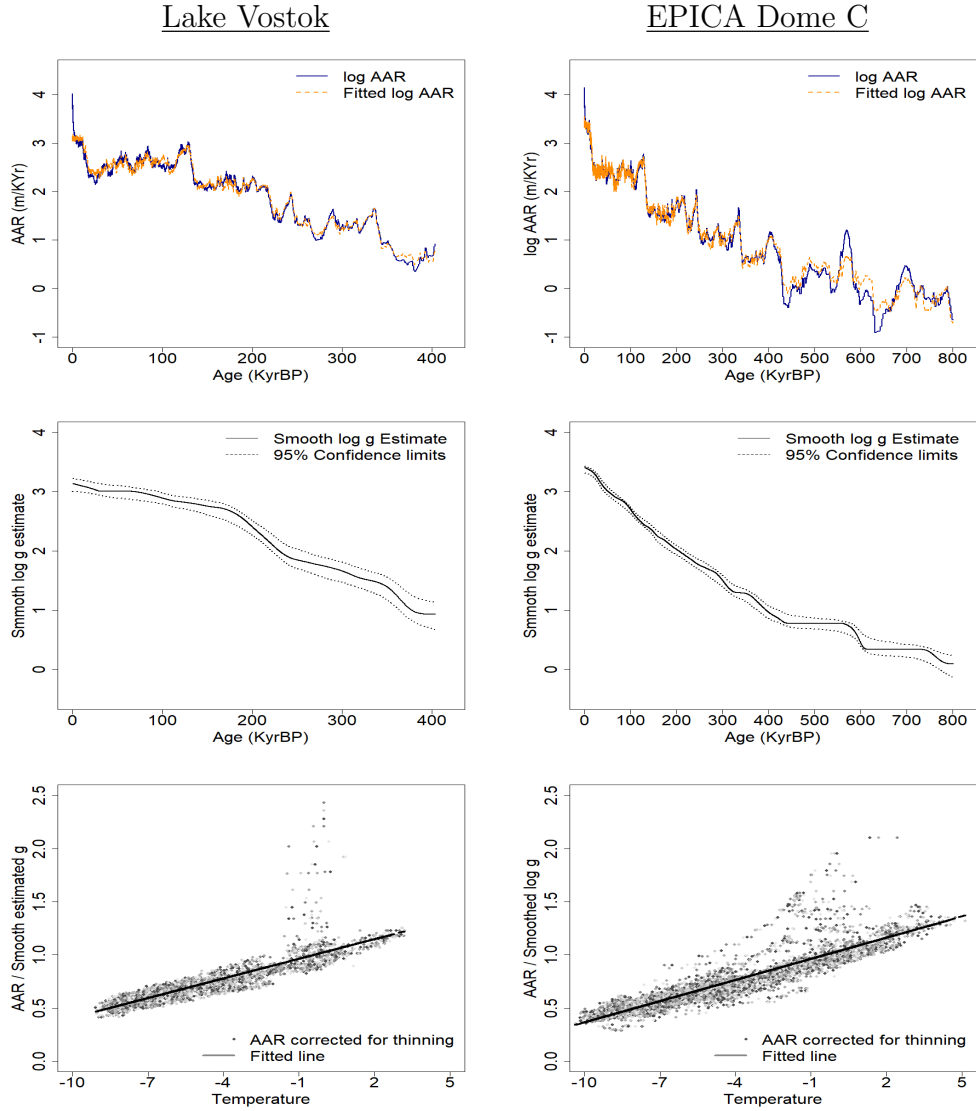


Figure 6: The top and middle row shows the plots of $\log AAR$ together with fitted $\log AAR$, and the plots of $\log \tilde{g}_n$ with pointwise bootstrap confidence intervals against age, respectively. The bottom row shows the scatter plot of $AAR - \tilde{g}$ against temperature along with the fitted line.

The bottom panel of Figure 6 shows that plots of the fitted AAR (adjusted for thinning) against temperature, for the two locations. The adjustment for thinning, based on model (3), is made by dividing AAR by the estimated function g . The line $1 + \tilde{\gamma}_n x$ is overlaid on the scatter as the “fitted line”. For Lake Vostok, the large departures from the fitted line occur in a few cases in the most recent samples (less than 1 KyrBP). For EPICA Dome C, there are some departures occurring in cycles at the distant past (see top panel). Apart from these systematic departures, which may be attributed to factors not included in the model, the points in the scatter plots stay very close to the fitted line. This indicates a persistently linear relationship with temperature disturbed at times by unaccounted factors.

7 Appendix

Proof of Theorem 1. By using (4), we can write

$$\begin{aligned}
Q_n(\gamma, g) &= \frac{1}{n} \sum_{i=1}^n [\log(1 + \gamma_0 x_i) - \log(1 + \gamma x_i) + \log g_0(z_i) - \log g(z_i)]^2 + \frac{1}{n} \sum_{i=1}^n \varepsilon_i^2 \\
&\quad + \frac{2}{n} \sum_{i=1}^n v_i \varepsilon_i + \frac{2}{n} \sum_{i=1}^n v'_i \varepsilon_i,
\end{aligned} \tag{15}$$

where $v_i = (\log(1 + \gamma_0 x_i) - \log(1 + \gamma x_i))$ and $v'_i = (\log g_0(z_i) - \log g(z_i))$, for $i = 1, 2, \dots, n$.

From Assumptions 1 and 2, the first term on the right hand side (RHS) of (15) can be viewed as the Riemann sum,

$$\frac{1}{\Delta} \sum_{i=1}^n [\log(1 + \gamma_0 x(d_i)) - \log(1 + \gamma x(d_i)) + \log g_0(z(d_i)) - \log g(z(d_i))]^2 \frac{\Delta}{n},$$

which converges to $Q(\gamma, g)$. The second term on RHS converges almost surely to $\frac{\sigma^2}{1-\phi^2}$, by

Lemma 1 given below. For the third term, note that

$$\frac{1}{n} \sum_{i=1}^n v_i \varepsilon_i = \frac{1}{n} \sum_{i=1}^n v_i \left(\sum_{j=0}^{i-1} \phi^j U_{i-j} + \phi^i \varepsilon_1 \right) = \frac{1}{n} \sum_{i=1}^n U_i \left(\sum_{j=i}^n v_j \phi^{j-i} \right) + \frac{\varepsilon_1}{n} \sum_{i=1}^n v_i \phi^i \quad (16)$$

Almost sure convergence of each of the two terms on the RHS of (16) to 0 follows from uniform boundedness of the sequence v_1, v_2, \dots, v_n and Lemma 2 given below. A similar line of argument together with the uniform boundedness of the sequence v'_1, v'_2, \dots, v'_n ensures almost sure convergence of the fourth term on RHS of (15) to 0. This completes the proof. \square

Lemma 1. *Let $\{\varepsilon_i\}_{1 \leq i \leq n}$ be a stationary autoregressive process satisfying Assumption 3. Then we have*

$$\lim_{n \rightarrow \infty} \frac{1}{n} \sum_{i=1}^n \varepsilon_i^2 = \frac{\sigma^2}{1 - \phi^2} \quad \text{with probability 1.} \quad (17)$$

Lemma 2. *Let $\{U\}_{1 \leq i \leq n}$ be a sequence of i.i.d. random variables such that $E(U_1) = 0$, $E(U_1^2) = \sigma^2$ and $E(U_1^4) < \infty$. Further let $|\phi| < 1$ and $\{v\}_{1 \leq i \leq n}$ be a sequence of real numbers such that $|v_i| < M$ for $i = 1, 2, \dots$. Then*

$$\lim_{n \rightarrow \infty} \frac{1}{n} \sum_{i=1}^n U_i \left(\sum_{j=i}^n v_j \phi^{j-i} \right) = 0, \quad \text{with probability 1.}$$

Lemma 1 and Lemma 2 can be proved using Borel-Cantelli lemma.

Proof of Theorem 2. The functional $Q(\gamma, g)$ defined on the parameter space $\Gamma \times \mathcal{G}$ is continuous with respect to the distance metric defined at the beginning of Section 3. Let $(\hat{\gamma}_{n_k}, \log \hat{g}_{n_k})$ be a subsequence of $(\hat{\gamma}_n, \log \hat{g}_n)$ that converges to the limit point $(\gamma', \log g')$. Then by using Theorem 1, we have

$$Q_{n_k}(\hat{\gamma}_{n_k}, \hat{g}_{n_k}) \xrightarrow{a.s.} Q(\gamma', g') + \frac{\sigma^2}{1 - \phi^2} \text{ as } n_k \rightarrow \infty$$

Since $\hat{\gamma}_{n_k}, \hat{g}_{n_k}$ minimizes Q_{n_k} , we have $Q_{n_k}(\hat{\gamma}_{n_k}, \hat{g}_{n_k}) \leq Q_{n_k}(\gamma, g)$ for all γ, g in the parameter space. Therefore,

$$\lim_{n_k \rightarrow \infty} Q_{n_k}(\gamma_{n_k}, g_{n_k}) \leq \lim_{n_k \rightarrow \infty} Q_{n_k}(\gamma_0, g_0) \stackrel{a.s.}{=} \frac{\sigma^2}{1 - \phi^2}.$$

This implies that $Q(\gamma', g') = 0$. Since Q has a unique minimum at (γ_0, g_0) , (γ', g') must coincide with (γ_0, g_0) . This completes the proof. \square

Proof of Theorem 3. Part (i): Note that

$$\begin{aligned} |\log \tilde{g}_n(z) - \log g_0(z)| &= \left| \frac{\frac{1}{nh} \sum_{i=1}^n K\left(\frac{z-z_i}{h}\right) [\log \hat{g}_n(z_i) - \log g_0(z)]}{\frac{1}{nh} \sum_{i=1}^n K\left(\frac{z-z_i}{h}\right)} \right| \\ &\leq \frac{\frac{1}{nh} \sum_{i=1}^n K\left(\frac{z-z_i}{h}\right) |\log \hat{g}_n(z_i) - \log g_0(z_i)|}{\frac{1}{nh} \sum_{i=1}^n K\left(\frac{z-z_i}{h}\right)} \\ &\quad + \left| \frac{\frac{1}{nh} \sum_{i=1}^n K\left(\frac{z-z_i}{h}\right) \log g_0(z_i)}{\frac{1}{nh} \sum_{i=1}^n K\left(\frac{z-z_i}{h}\right)} - \log g_0(z) \right|. \end{aligned} \quad (18)$$

From Theorem 2, we have

$$\sup_z |\log \hat{g}_n(z) - \log g_0(z)| \rightarrow 0 \text{ almost surely,} \quad (19)$$

i.e., for an arbitrary $\eta > 0$ there exists a (possibly random) positive integer $N(\eta)$ such that

$$\sup_z |\log(\hat{g}_n(z)) - \log(g_0(z))| < \eta \text{ for all } n \geq N(\eta) \text{ with probability 1.} \quad (20)$$

Therefore, the first term on the RHS of (18) converges uniformly over z almost surely. The second term is non-random. By using first-order Taylor series expansion of $\log g_0(z_i)$ around z , we have

$$\log g_0(z_i) = \log g_0(z) + \frac{g_0'(\xi_i)}{g_0(\xi_i)}(z_i - z), \quad (21)$$

for some $\xi_i \in (z_i, z)$. According to (5), g'_0 bounded. Further, g_0 is assumed to be bounded away from zero. Therefore, we have

$$\left| \frac{g'_0(z)}{g_0(z)} \right| \leq C_{g_0} \quad (22)$$

for some constant C_{g_0} . Thus, the second term on the RHS of (18) is bounded as

$$\left| \frac{\sum_{i \in \{1, 2, \dots, n\}: |z - z_i| < h} K\left(\frac{z - z_i}{h}\right) \frac{g'_0(\xi_i)}{g_0(\xi_i)} (z_i - z)}{\sum_{i \in \{1, 2, \dots, n\}: |z - z_i| < h} K\left(\frac{z - z_i}{h}\right)} \right| \leq C_{g_0} h \text{ uniformly over } z,$$

which goes to zero as $h \rightarrow 0$. This completes the proof of part (i).

Part (ii): We can expand $\tilde{Q}_n(\gamma) = \frac{1}{n} \sum_{i=1}^n (y_i - \log \tilde{g}_n(z_i) - \log(1 + \gamma x_i))^2$ as follows.

$$\begin{aligned} \tilde{Q}_n(\gamma) &= \frac{1}{n} \sum_{i=1}^n \varepsilon_i^2 + \frac{1}{n} \sum_{i=1}^n [\log g_0(z_i) - \log \tilde{g}_n(z_i)]^2 + \frac{1}{n} \sum_{i=1}^n [\log(1 + \gamma_0 x_i) - \log(1 + \gamma x_i)]^2 \\ &\quad + \frac{2}{n} \sum_{i=1}^n \varepsilon_i [\log g_0(z_i) - \log \tilde{g}_n(z_i)] + \frac{2}{n} \sum_{i=1}^n \varepsilon_i [\log(1 + \gamma_0 x_i) - \log(1 + \gamma x_i)] \\ &\quad + \frac{2}{n} \sum_{i=1}^n [\log g_0(z_i) - \log \tilde{g}_n(z_i)] [\log(1 + \gamma_0 x_i) - \log(1 + \gamma x_i)]. \end{aligned} \quad (23)$$

We will establish the convergence of each term on the RHS of (23). The almost sure convergence of the first term to $\frac{\sigma^2}{1 - \phi^2}$ follows directly from Lemma 1. The second term converges almost surely to 0 by virtue of Part (i), since

$$\left| \frac{1}{n} \sum_{i=1}^n [\log g_0(z_i) - \log \tilde{g}_n(z_i)]^2 \right| \leq \sup_z |\log g_0(z) - \log \tilde{g}_n(z)|^2. \quad (24)$$

From Assumption 2, the third term on the RHS of (23) can be viewed as the Riemann sum

which converges as follows.

$$\begin{aligned} \frac{1}{\Delta} \lim_{n \rightarrow \infty} \sum_{i=1}^n \left[\log \left(1 + \gamma_0 x \left(\frac{i\Delta}{n} \right) \right) - \log \left(1 + \gamma x \left(\frac{i\Delta}{n} \right) \right) \right]^2 \frac{\Delta}{n} \\ = \frac{1}{\Delta} \int_0^\Delta [\log(1 + \gamma_0 x(w)) - \log(1 + \gamma x(w))]^2 dw. \end{aligned}$$

As for the fourth term, note that

$$\left| \frac{2}{n} \sum_{i=1}^n \varepsilon_i [\log g_0(z_i) - \log \tilde{g}_n(z_i)] \right| \leq 2 \sup_z |\log g_0(z) - \log \tilde{g}_n(z)| \times \frac{1}{n} \sum_{i=1}^n |\varepsilon_i|. \quad (25)$$

The first factor on the RHS of (25) converges almost surely to 0, by virtue of Part (i). The second factor converges to $E(|\varepsilon_1|)$ almost surely by using a similar argument as in Lemma 1. Thus, the product of the two factors converges to 0 almost surely. The fifth term on the RHS of (23) is identical to the third term on the RHS of (15), which has already been shown to converge almost surely to 0. Finally, the sixth term reduces, due to the boundedness of $\log(1 + \gamma x_i)$, to

$$\left| \frac{2}{n} \sum_{i=1}^n [\log g_0(z_i) - \log \tilde{g}_n(z_i)] [\log(1 + \gamma_0 x_i) - \log(1 + \gamma x_i)] \right| \\ \leq 2 \sup_z |\log g_0(z) - \log \tilde{g}_n(z)| \times \sup_{x, \gamma} |\log(1 + \gamma_0 x_i) - \log(1 + \gamma x_i)|, \quad (26)$$

which converges to 0 almost surely by Part (i). Thus, we have

$$\lim_{n \rightarrow \infty} \tilde{Q}_n(\gamma) = \frac{\sigma^2}{1 - \phi^2} + \frac{1}{\Delta} \int_0^\Delta [\log(1 + \gamma_0 x(w)) - \log(1 + \gamma x(w))]^2 dw, \text{ almost surely.} \quad (27)$$

The almost sure convergence of $\tilde{\gamma}_n = \arg \min_{\gamma \in \Gamma} \tilde{Q}_n(\gamma)$ to γ_0 follows along the lines of the proof of Theorem 2. This completes the proof of Part (ii). \square

Proof of Theorem 4. Part (i): From (13), we have

$$\tilde{\phi}_n = \frac{\frac{1}{n} \sum_{i=2}^n [T_n(x_i, z_i) T_n(x_{i-1}, z_{i-1}) + T_n(x_i, z_i) \varepsilon_{i-1} + T_n(x_{i-1}, z_{i-1}) \varepsilon_i + \varepsilon_i \varepsilon_{i-1}]}{\frac{1}{n} \sum_{i=2}^n (T_n^2(x_i, z_i) + \varepsilon_i^2 + 2T_n(x_i, z_i) \varepsilon_i)}, \quad (28)$$

where

$$\begin{aligned} T_n(x_i, z_i) &= \log(1 + \gamma_0 x_i) - \log(1 + \tilde{\gamma}_n x_i) + \log g_0(z_i) - \log \tilde{g}_n(z_i) \\ &= -\log\left(1 + \frac{\tilde{\gamma}_n - \gamma_0}{1 + \gamma_0 x_i}\right) + \log g_0(z_i) - \log \tilde{g}_n(z_i). \end{aligned} \quad (29)$$

We have, by the continuity and monotonicity of the log function,

$$\begin{aligned} |T_n(x_i, z_i)| &\leq \sup_x \left| \log\left(1 + \frac{\tilde{\gamma}_n - \gamma_0}{1 + \gamma_0 x}\right) \right| + \sup_z |\log g_0(z) - \log \tilde{g}_n(z)| \\ &= \left| \log\left(1 + \frac{\tilde{\gamma}_n - \gamma_0}{\inf_x(1 + \gamma_0 x)}\right) \right| + \sup_z |\log g_0(z) - \log \tilde{g}_n(z)| \end{aligned} \quad (30)$$

The RHS of (30) converges to 0 almost surely under Assumption 2, by virtue of Part(i) and Part (ii) of Theorem 3.

The numerator on the RHS of (28) is decomposed into four terms. The first term reduces to

$$\left| \frac{1}{n} \sum_{i=2}^n T_n(x_i, z_i) T_n(x_{i-1}, z_{i-1}) \right| \leq \sup_{x,z} |T_n(x, z)|^2, \quad (31)$$

which goes to 0 almost surely. The second term of the numerator reduces to

$$\left| \frac{1}{n} \sum_{i=2}^n T_n(x_i, z_i) \varepsilon_{i-1} \right| \leq \sup_{x,z} |T_n(x, z)| \times \frac{1}{n} \sum_{i=2}^n |\varepsilon_{i-1}|, \quad (32)$$

which goes to $0 \times E(|\varepsilon_1|)$ or 0 almost surely, as argued in the case of (25). A similar argument establishes that the third term of the numerator converges to 0 almost surely.

The fourth term is

$$\frac{1}{n} \sum_{i=2}^n \varepsilon_i \varepsilon_{i-1} = \frac{1}{n} \sum_{i=2}^n (U_i + \phi \varepsilon_{i-1}) \varepsilon_{i-1} = \frac{1}{n} \sum_{i=2}^n \phi \varepsilon_{i-1}^2 + \frac{1}{n} \sum_{i=2}^n U_i \varepsilon_{i-1}. \quad (33)$$

From Lemma 1, the first term on the RHS of (33) converges almost surely to $\phi \frac{\sigma^2}{1-\phi^2}$. The second term is $\frac{1}{n} \sum_{i=2}^n W_i$, where $W_i = U_i \varepsilon_{i-1}$ for $i = 2, 3, \dots, n$. Note that U_i is

independent of ε_{i-1} and $E(W_i) = E(U_i)E(\varepsilon_{i-1}) = 0$ for $i = 2, 3, \dots, n$. By using a similar line of argument as in Lemma 1 and the Borel-Cantelli lemma, it can be shown that $\frac{1}{n} \sum_{i=2}^n W_i \rightarrow 0$ almost surely. Thus, the numerator on the RHS of (28) converges to $\phi \frac{\sigma^2}{1-\phi^2}$ with probability 1. The denominator on RHS of (28) is found to converge to $\frac{\sigma^2}{1-\phi^2}$ almost surely, through a similar line of argument. This completes the proof of Part (i).

Part (ii): From (14), we have

$$\tilde{\sigma}_n^2 = \frac{1}{n} \sum_{i=2}^n \tilde{\varepsilon}_i^2 + \tilde{\phi}_n^2 \frac{1}{n} \sum_{i=2}^n \tilde{\varepsilon}_{i-1}^2 - 2\tilde{\phi}_n \frac{1}{n} \sum_{i=2}^n \tilde{\varepsilon}_i \tilde{\varepsilon}_{i-1} \quad (34)$$

Each of the terms $\frac{1}{n} \sum_{i=2}^n \tilde{\varepsilon}_i^2$ and $\frac{1}{n} \sum_{i=2}^n \tilde{\varepsilon}_{i-1}^2$ converges almost surely to $\frac{\sigma^2}{1-\phi^2}$, through an argument similar to that used for the denominator on the RHS of (28). Likewise, the term $\frac{1}{n} \sum_{i=2}^n \tilde{\varepsilon}_i \tilde{\varepsilon}_{i-1}$ converges to $\phi \frac{\sigma^2}{1-\phi^2}$ almost surely by an argument similar to that used for the numerator on RHS of (28). These convergences, together with Part (i), establish the almost sure convergence of the RHS of (34) to σ^2 .

□

References

- Algarra, I., Nieto, R., Ramos, A. M., Eiras-Barca, J., Trigo, R. M., and Gimeno, L. (2020). Significant increase of global anomalous moisture uptake feeding landfalling atmospheric rivers. *Nature Communications*, **11**(1), 2041–1723.
- Allan, R. P. and Soden, B. J. (2008). Atmospheric warming and the amplification of precipitation extremes. *Science*, **321**(5895), 1481–1484.
- Barlow, R., Brunk, H., Bartholomew, D., and Bremner, J. (1972). *Statistical Inference*

Under Order Restrictions: The Theory and Application of Isotonic Regression. Wiley series in probability and mathematical statistics. John Wiley & Sons.

Bazin, L., Landais, A., Lemieux-Dudon, B., Toyé Mahamadou Kele, H., Veres, D., Parrenin, F., Martinerie, P., Ritz, C., Capron, E., Lipenkov, V. Y., Loutre, M.-F., Raynaud, D., Vinther, B. M., Svensson, A. M., Rasmussen, S. O., Severi, M., Blunier, T., Leuenberger, M. C., Fischer, H., Masson-Delmotte, V., Chappellaz, J. A., and Wolff, E. W. (2013). An optimized multi-proxy, multi-site antarctic ice and gas orbital chronology (aicc2012): 120-800 ka. *Climate of the Past*, **9**(4), 1715–1731.

DiCiccio, T. J. and Efron, B. (1996). Bootstarp confidence interval. *Statistical Science*, **11**, 189–228.

Efron, B. and Tibshirani, R. J. (1993). *An Introduction to Bootstrap*. Chapman and Hall CRC, Florida, USA.

Ghosh, A. K. and Chaudhuri, P. (2004). Optimal smoothing in kernel discriminant analysis. *Statistica Sinica*, **14**(2), 457–483.

Härdle, W. (1990). *Applied Nonparametric Regression*. Cambridge University Press, Cambridge, England.

Jennrich, R. I. (1969). Asymptotic properties of non-linear least squares estimators. *The Annals of Mathematical Statistics*, **40**(2), 633–643.

Jouzel, J. and Masson-Delmotte, V. (2007). EPICA Dome C Ice Core 800KYr deuterium data and temperature estimates. Supplement to: Jouzel, Jean et al. (2007): Orbital and millennial Antarctic climate variability over the past 800,000 years. *Science*, 317(5839), 793-797.

- Lahiri, S. N. (2003). *Resampling methods for dependent data*. Springer, New York.
- Luss, R., Rosset, S., and Shahar, M. (2012). Efficient regularized isotonic regression with application to gene–gene interaction search. *Annals of Applied Statistics*, **6**(1), 253–283.
- Niculescu-Mizil, A. and Caruana, R. (2005). Predicting good probabilities with supervised learning. *Proceedings of the 22nd international conference on Machine learning*.
- Parrenin, F., Barnola, J.-M., Beer, J., Blunier, T., Castellano, E., Chappellaz, J., Dreyfus, G., Fischer, H., Fujita, S., Jouzel, J., Kawamura, K., Lemieux-Dudon, B., Loulergue, L., Masson-Delmotte, V., Narcisi, B., Petit, J.-R., Raisbeck, G., Raynaud, D., Ruth, U., Schwander, J., Severi, M., Spahni, R., Steffensen, J. P., Svensson, A., Udisti, R., Waelbroeck, C., and Wolff, E. (2007). The edc3 chronology for the epica dome c ice core. *Climate of the Past*, **3**(3), 485–497.
- Petit, J. R., Jouzel, J., Raynaud, D., Barkov, N. I., Barnola, J.-M., Basile, I., Bender, M., Chappellaz, J., Davis, M., Delaygue, G., Delmotte, M., Kotlyakov, V. M., Legrand, M., Lipenkov, V. Y., Lorius, C., PÉpin, L., Ritz, C., Saltzman, E., and Stievenard, M. (1999). Climate and atmospheric history of the past 420,000 years from the Vostok ice core, Antarctica. *Nature*, **399**(6735), 429–436.
- Rapp, D. (2019). *Ice Core Data*, pages 83–118. Springer International Publishing, Cham.
- Scambos, T. and Shuman, C. (2016). Comment on ‘mass gains of the antarctic ice sheet exceed losses’ by h. j. zwally and others. *Journal of Glaciology*, **62**(233), 599–603.
- Sen, B., Banerjee, M., and Woodroffe, M. (2010). Inconsistency of bootstrap: The grenander estimator. *Annals of Statistics*, **38**, 1953–1977.

- Siegert, M. J. (2003). Glacial–interglacial variations in central east antarctic ice accumulation rates. *Quaternary Science Reviews*, **22**, 741–750.
- Sreelekshmy, S. (2023). *A Study on Paleoclimatic Ice-core Data: Statistical Modelling of Accumulation Rate*. PhD Thesis, IIT Bombay.
- Wang, P. K. (2013). *Physics and dynamics of clouds and precipitation*. Cambridge University Press, Cambridge, England.
- Zwally, H. J., Li, J., Robbins, J. W., Saba, J. L., Yi, D., and Brenner, A. C. (2015). Mass gains of the antarctic ice sheet exceed losses. *Journal of Glaciology*, **61**(230), 1019–1036.